CIRP Annals - Manufacturing Technology 00 (2020) 1–4

Contents lists available at ScienceDirect

CIRP Annals - Manufacturing Technology

journal homepage: https://www.editorialmanager.com/CIRP/default.aspx

Prediction of local sintering in laser beam machining of green Y-TZP ceramic

François Ducobu[a,*], Edouard Rivière-Lorphèvre[a], Anthonin Demarbaix[a], Bert Lauwers (1)[b]

[a] Machine Design and Production Engineering Lab, Faculty of Engineering of the University of Mons, Mons, Belgium
[b] Department of Mechanical Engineering, KU Leuven & Member Flanders Make Leuven, Belgium

ARTICLE INFO

Article history:
Available online xxx

Keywords:
Laser beam machining (LBM)
Ceramic
Thermal effects

ABSTRACT

Laser beam machining of Y-TZP engineering ceramic material is carried out in green stage to increase the material removal rate. The generation of hot spots may cause local sintering of the ceramic material leading to a decrease of the mechanical properties of the final sintered component. This paper presents the implementation of alternative laser beam paths to reduce the hot spots occurrence. A thermal finite element model has been developed to support the experimental analysis as well as the prediction of local sintering. The experimental validation of the newly developed toolpath strategies confirmed the reduction of local sintering.

1. Introduction

Amongst engineering ceramics, Yttria-stabilised Tetragonal Zirconia Polycrystal (Y-TZP) exhibits a high fracture toughness and a high flexural strength, making it suitable for a wide range of applications [1–3]. Compared to bisque and fired machining [4], green machining allows a much easier and higher material removal rate. However, the low mechanical properties and high brittleness of a green blank often induce brittle fracture as well as crack initiation and propagation during tool interaction [4]. To avoid material-tool contact, laser beam machining of ceramics materials in its green state is studied in this research. Material removal rate is further increased thanks to a patented blank preparation [5], including an additive favouring material removal as well as a faster laser machining process. A TA Instrument EM-1600 DLF-2 is used to experimentally measure, based on the flash method, the thermal diffusivity, α (2.3E-7 m^2/s), and the specific heat, C_p (553.6 J/kgK), of the green Y-TZP ceramic (at 20 °C). The thermal conductivity, k (0.43 W/mK), is then computed with the measured density, ρ (3283 kg/m^3): $k = \alpha\rho C_p$.

Laser beam machining of ceramics in green state is not commonly applied. It introduces the generation of hot spots, which are volumes of material that are heated more than required. These hot spots can locally sinter the material, leading to a decrease of the mechanical properties of the final sintered component and to an uncontrolled material removal rate (usually an excessive material removal on the current layer and the impossibility to remove, with the same laser parameters, the material on the next layers). Therefore, these hot spots must be avoided.

Numerical modelling of the laser beam machining process can be carried out with finite element methods [6]. Most of the models predict the temperature fields for classical materials. Only few thermal finite element models are found for laser beam machining of ceramic materials. None of them deals with green Y-TZP machining, nor the influence of laser beam paths [1,6].

This paper introduces various laser beam path strategies and a method, based on thermal finite element modelling, to reduce, but also predict, the hot spots generation and thus local sintering.

2. Development of laser beam strategies

2.1. Overview of applied laser beam strategies

The usual toolpath strategy in laser beam machining is the ZIG strategy [7]: the current layer is machined unidirectionally and the next layer is rotated by a given angle (usually 90° [7]). To reduce the machining time and minimise the generation of hot spots during the interaction of the laser beam and the material, two alternative toolpath strategies are introduced: the ZIG-ZAG and the CONTOUR toolpath strategies, which are commonly used in milling operations. Fig. 1 shows the three machining strategies in case of 2D pocket laser machining and without transverse overlap: $O_T = \frac{2}{\pi}\cos^{-1}\left(\frac{h_d}{d}\right) - \frac{h_d}{2\pi}\sqrt{d-h_d} = 0\%$ with d the spot diameter and h_d the hatch distance.

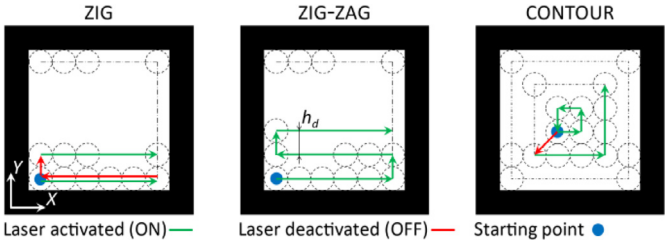

Fig. 1. Laser beam strategies (for a transverse overlap O_T of 0%).

* Corresponding author.
E-mail address: Francois.Ducobu@umons.ac.be (F. Ducobu).

https://doi.org/10.1016/j.cirp.2020.04.051
0007-8506/

The ZIG strategy, being the usual toolpath strategy in laser beam machining, is the reference. With it, a significant portion of the operation is performed with the laser deactivated. In the ZIG-ZAG strategy, the laser is always activated leading to a longer stay of the beam at the bifurcations (i.e. where the beam changes direction). The CONTOUR strategy follows the contours of the machined feature, from the inside to the outside. The contour of the feature is machined consecutively with a scale factor and the laser is deactivated when it moves from one contour to the other.

2.2. Thermal finite element model

The comparison of the three strategies in terms of hot spots generation is performed with the help of a simplified thermal finite element model. The model does not take the ablation of the material into account (no phase change and no material removal). This numerical model is developed within the Abaqus/Standard software and provides the transient thermal fields induced by the laser beam. The laser beam is modelled as a moving heat source through a DFLUX subroutine. The laser spot geometry (i.e. a circle) is approximated by a square of equivalent surface as the finite elements shape is a brick [8]. As the heat source modelling is critical for an accurate temperature prediction [1], it is modelled as a three-dimensional conical source which is the most flexible source model to represent reality [9]. The laser parameters are provided in Table 1.

Table 1
Laser parameters.

Laser parameter	Value
Laser power, P	20 W
Spot diameter, d	50 μm
Scanning speed, laser activated, v_{ON}	800 mm/s
Scanning speed, laser deactivated, v_{OFF}	5000 mm/s

The finite element model is first validated in the simplified configuration of the Wilson-Rosenthal equation [10]. It represents the temporal evolution of the temperature, T, at a point of space while the heat source of power P is moving in the positive X direction:

$$T = T_\infty + \frac{P \in}{2\pi k L} e^{-\frac{|v_{ON}|}{2\alpha}(L+x)}$$

with T_∞ the ambient temperature, $\in$ the power fraction absorbed by the material, L the distance between the heat source and the point of space, x the horizontal distance between the heat source and the point of space.

Fig. 2(a) shows the green Y-TZP blank for the model validation. This validation is carried out by comparing the integral of the temporal evolution of the temperature at one node. The finite element model is composed of approximately 112,000 hexahedral elements (8-node bricks). The element edge size is 10 μm, which is in accordance with a mesh convergence study aiming at an integral value independent of the mesh size, while keeping the computation time low. The node at which the temperature evolution is considered is located in the middle of the blank at a depth of 37.5 μm (i.e. the average thickness of the layer removed by the laser). The difference between the analytical and the numerical integrals is 10.6%, which is low enough to validate the model taking into account that some of the analytical solution hypotheses differ from these of the finite element model. For example, the heat source is assumed to be punctual although there is spot diameter given in the model. This implies that finite element model results are more a guideline rather than an absolute result. The low discrepancy between the analytical reference and the numerical model allows validation in this study.

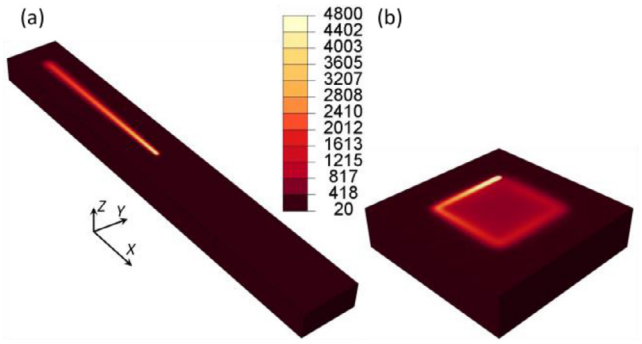

Fig. 2. Examples of finite element temperature contours (in °C) (a) Validation model when the heat source reaches the half length of the blank (b) CONTOUR strategy when the heat source is at the end of the beam path.

2.3. Comparison of laser beam strategies

The three laser beam strategies are implemented in the finite element model through DFLUX subroutines. A square surface of 1 mm × 1 mm (Fig. 2(b)) in the middle of a green Y-TZP blank of 2 mm (X) × 2 mm (Y) × 0.5 mm (Z) composed of approximatively 230, 000 elements is heated. These dimensions are chosen to avoid the influence of the blank boundaries on the results. A single layer, the top surface of the blank, is heated.

To compare the impact of each strategy on the generation of hot spots, a normalised temperature T^*_{node} is defined:

$$T^*_{node} = \frac{T_{node}}{T_{max,zig}}$$

with T_{node} the node temperature and $T_{max,zig}$ the maximal temperature recorded with the ZIG strategy. The maximal value of the normalised temperature is then plotted at each node to obtain a map of the maximal temperatures reached during the machining of the whole surface as shown in Fig. 3.

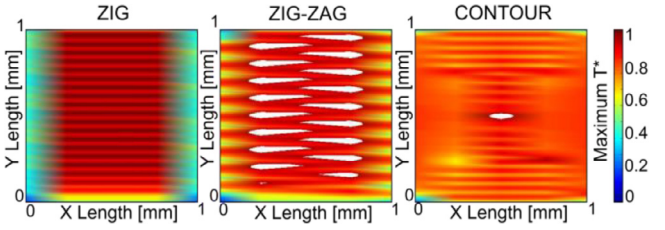

Fig. 3. Maximal normalised temperature map of the 1 mm × 1 mm heated surface for the three laser beam strategies (in a white zone: $T^*_{node} > 1$); the heat source starts from the bottom left corner for the ZIG and ZIG-ZAG strategies.

Many zones with a maximal normalised temperature higher than 1 are observed for the ZIG-ZAG strategy, as well as an additional heat accumulation on the lateral sides of the pocket in comparison to the ZIG strategy. The heat accumulation is more diffuse for the CONTOUR strategy and the temperature level is globally lower and more uniform, but a high temperature zone is observed in the middle of the pocket. In terms of machining time, in comparison to the ZIG reference (27.4 ms), the ZIG-ZAG is the fastest (9.1% reduction), while the CONTOUR is the second fastest (8.4% reduction). This is due to the reduction of the length travelled by the laser when it is deactivated.

Although the ZIG-ZAG strategy is the fastest, it leads to high temperatures, larger than in the ZIG strategy ($T^*_{node} > 1$). The high temperatures are located away from the pocket sides just after bifurcations. This is due to the passage of the laser beam in an area very close to that before its change of trajectory, where the material does not have the time to dissipate the accumulated energy.

In the CONTOUR strategy, the same phenomenon occurs at the beginning of the toolpath, thus at the centre of the pocket. As the heating source moves away, the heat accumulation is less important. The hot spots generated by the CONTOUR strategy are therefore localised on a small area at the centre of the pocket and the global temperature level is lower compared to the ZIG strategy.

Based on this numerical study, the CONTOUR strategy should be favoured to reduce the generation of hot spots. In addition, the machining time is also reduced compared to the ZIG strategy. The developed

Please cite this article as: F. Ducobu et al., Prediction of local sintering in laser beam machining of green Y-TZP ceramic, CIRP Annals - Manufacturing Technology (2020), https://doi.org/10.1016/j.cirp.2020.04.051

finite element model can be used in future to develop other new and innovative laser beam strategies aiming at both the avoidance of hot spots and machining time reduction.

3. Prediction of local sintering

In this section, a developed procedure is described to detect and predict the local sintering trend. Both the reference ZIG and the introduced CONTOUR strategies are considered.

3.1. Experimental study

The blanks (blocks of 66 mm (X) × 66 mm (Y) × 15 mm (Z)) of green Y-TZP are manufactured under patent [5] by the Belgian Ceramic Research Centre (BCRC). The laser beam machining is performed with an IPG nanosecond fibre laser of YLP V2 1 100 100 100 type. As in the finite element model, a single layer of 1 mm × 1 mm is machined (in green state).

The evaluation of the fraction of the machined surface that is locally sintered (Fig. 4) is performed by an in-house developed image processing software. A picture of the machined surface is taken with a HIROX KH-8700 Digital Optical Microscope. This image is then converted to greyscale in which the lighter pixels represent local sintering. A threshold value is calibrated to determine local sintering and artefacts are deleted. The number of detected pixels is finally counted to obtain the fraction of the surface that is sintered. The sintered pixels are converted in black for visualisation purposes.

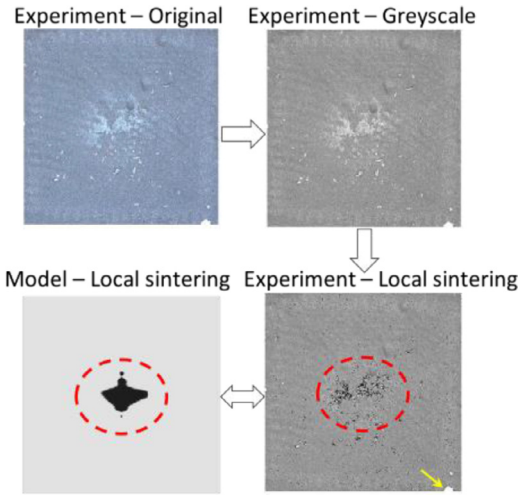

Fig. 4. Example of local sintering for the 1 mm × 1 mm machined surface with the contour strategy. Three experimental steps and numerical result; the main sintered area is circled in red and the yellow arrow points to one of the artefacts observed in the experiments that is removed from the detection. (For interpretation of the references to colour in this figure legend, the reader is referred to the web version of this article.)

The percentage of sintered surface with the ZIG toolpath is 3.3%, while 2.1% for the proposed CONTOUR toolpath. It means that the alternative CONTOUR tool path strategy reduces the local sintering by 36%. This also confirms the finite element prediction of the reduction of hot spots generation.

3.2. Scanning speed influence on local sintering

The image processing software is applied to the results of the finite element model and the experimental results to detect and predict the local sintering when the laser machining parameters are modified. Seven scanning speeds are used (Table 2).

A two-step procedure is followed for the numerical model as it does not take material ablation into account. First, based on the map of the maximal normalised temperatures, a temperature threshold, T_s, is calibrated to determine the area where local sintering may occur. When the threshold temperature is reached at one node, it is assumed that local sintering occurs at that node and a two-colour sintering risk map is obtained (Fig. 4). It is important to stress that this temperature is a fictive temperature because of the simplifications of the finite element model. In a second step, the percentage of sintering in this map is computed. This numerical percentage of sintered surface, S_{loc}, sim., is compared to the experimental one, S_{loc}, exp.

Table 2
Local sintering, S_{loc}, with the variation of the scanning speed, v_{ON}; reference speed in bold.

v_{ON} (mm/s)	S_{loc}, exp. (%)	S_{loc}, sim. (%)	S_{loc}, cal. sim. (%)
600	4.1	83.6	4.2
700	3.9	28.1	3.8
800	**2.1**	**2.1**	**2.1**
900	1.4	0.2	1.5
1000	1.4	0.2	1.3
1100	1.5	0.2	1.4
1200	1.4	0.2	1.4

S_{loc}, exp.: experimental value of local sintering, S_{loc}, sim.: numerical value of local sintering with the threshold temperature calibrated for the reference scanning speed (800 mm/s), S_{loc}, cal. sim.: numerical value of local sintering with the threshold temperature calibrated for the each scanning speed.

The procedure is first applied to the reference machining conditions (v_{ON} = 800 mm/s). The calibration of the threshold temperature, based on the experimental result to obtain the same fraction of local sintering, leads to a fictive temperature of 2621 °C. The numerical model is then used to predict the percentage of sintering when the scanning speed varies, S_{loc}, sim. Table 2 compares the numerical and experimental values. The general trend is globally well captured by the model: the local sintering decreases with increasing scanning speed until 800 mm/s. Then, it reaches a more or less constant value. The values of sintering are however different between the experiments and the modelling. This shortcoming of the model is directly linked to its hypotheses. The calibration of the threshold temperature on a single test is therefore not enough.

The temperature calibration is consequently extended to the other scanning speeds. This brings the numerical values, S_{loc}, cal. sim., to the level of the experimental values, S_{loc}, exp. (Table 2). The evolution of the temperature threshold with the scanning speed is plotted in Fig. 5. It follows an exponential tendency, $T_s = 5871.6\ e^{-1.0E-3\ v_{ON}}$, with a correlation coefficient R^2 of 99%, which is a finding of this study.

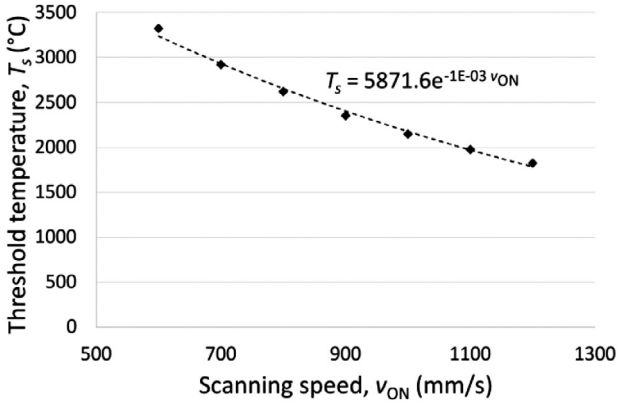

Fig. 5. Threshold temperature versus the scanning speed for the finite element model and the CONTOUR strategy.

The threshold temperature is an image of the energy that is transferred to the material. An increase of energy increases the local sintering because a larger volume is thermally impacted by the laser beam, while not all the material is removed. A higher threshold temperature will therefore lead to a larger amount of local sintering. In Fig. 5, the temperature threshold increases when the interaction between the laser beam and the material is longer (i.e. when the

Please cite this article as: F. Ducobu et al., Prediction of local sintering in laser beam machining of green Y-TZP ceramic, CIRP Annals - Manufacturing Technology (2020), https://doi.org/10.1016/j.cirp.2020.04.051

scanning speed decreases). This is because the energy transferred to the material is larger, resulting in an increased risk of local sintering (Table 2). It is noted that the risk of local sintering is now accurately modelled. As previously highlighted, the absolute value of the threshold temperature has no physical meaning because it is a fictive temperature.

3.3. Influence of the laser beam overlap on local sintering

Based on the results of the influence of the scanning speed on the local sintering, the procedure is now extended to perform the prediction of the local sintering when the transverse overlap varies. Six transverse overlap values are used (Table 3).

Table 3
Local sintering, S_{loc}, with the variation of the transverse overlap, O_T for v_{ON} = 800 mm/s; calibration overlaps in bold.

O_T (%)	S_{loc}, exp. (%)	S_{loc}, sim. (%)
10	**1.1**	**1.1**
20	2.2	0.7
30	1.6	0.3
40	**2.1**	**2.1**
50	4.3	8.0
60	4.4	16.2

S_{loc}, exp.: experimental value of local sintering, S_{loc}, sim.: numerical value of local sintering with the threshold temperature calibrated for the calibration transverse overlaps (10% and 40%).

It is assumed that an exponential correlation also relates the temperature threshold and the transverse overlap. The calibration of the temperature threshold is performed for two machining conditions to obtain the exponential link between the transverse overlap and the threshold temperature. The first temperature corresponds to the reference conditions with an overlap of 40%. The second temperature is calibrated for the lower boundary of the overlap range, 10%. The exponential relation is $T_s = 1736.8\ e^{10.3E\text{–}3\ O_T}$.

Table 3 presents the comparison between the numerical prediction and the experimental measurements. It shows that the model predicts accurately the experimental trend: the local sintering globally increases with the transverse overlap. Outside the calibration range, the predicted value is overestimated. This allows the model to predict qualitatively the influence of the machining parameters on the local sintering and confirms the exponential correlation hypothesis.

4. Conclusions

This paper presents the introduction of two alternative laser beam paths, ZIG-ZAG and CONTOUR, to reduce the generation of hot spots that can lead to a local sintering of the machined green Y-TZP ceramic. The risk of local sintering is predicted by a thermal finite element model of a moving heat source and is experimentally confirmed.

A procedure is developed to estimate the fraction of local sintering of the machined surface. This method is applied to both experimental and numerical results, allowing to validate the results of the finite element model. The local sintering is predicted with this model with a good qualitative agreement in adequation with its hypotheses. Both the scanning speed and the transverse overlap exhibit an exponential correlation with the threshold temperature linked to the local sintering. This reduces the number of calibration experiments to two. The results of this study show that the introduced CONTOUR laser strategy should be favoured to (i) reduce the fraction of local sintering by 36% and (ii) reduce the machining time by 8.4% by comparison to the ZIG strategy, the latter taken as reference. Values of local sintering as low as 1% of the machined surface are obtained for the conditions of this study.

The developed method/procedure can be used in the future to optimise the machining parameters in order to avoid the risk of local sintering while reducing the machining time. New and innovative laser beam strategies aiming at the same objectives can be developed based on the same procedures.

References

[1] Ferraris E, Vleugels J, Guo Y, Bourell D, Kruth JP, Lauwers B (2016) Shaping of Engineering Ceramics by Electro, Chemical And Physical Processes. *CIRP Annals - Manufacturing Technology* 65:761–784.
[2] Kizaki T, Harada K, Mitsuishi M (2014) Efficient and Precise Cutting of Zirconia Ceramics Using Heated Cutting Tool. *CIRP Annals - Manufacturing Technology* 63:105–108.
[3] Yan J, Okuuchi T (2019) Chip Morphology and Surface Integrity in Ultraprecision Cutting of Yttria-Stabilized Tetragonal Zirconia Polycrystal. *CIRP Annals - Manufacturing Technology* 68:53–56.
[4] El-Wardany T, Barth R, Holowczak J, Tredway W, Chen LJ (2009) Optimum Process Parameters to Produce Green Ceramic Complex Parts. *CIRP Annals - Manufacturing Technology* 58:109–112.
[5] F. Petit, V. Lardot, C. Ott, E. Juste, F. Cambier, Ceramic Particle Mixture, and Method for Manufacturing Ceramic Parts from Such a Mixture, WO/2012/64025, 2014.
[6] Parandoush P, Hossain A (2014) A Review of Modeling and Simulation of Laser Beam Machining. *International Journal of Machine Tools and Manufacture* 85:135–145.
[7] Heyl P, Olschewski T, Wijnaendts RW (2001) Manufacturing of 3D Structures for Micro-Tools Using Laser Ablation. *Microelectronic Engineering* 57–58:775–780.
[8] Demarbaix A, Ducobu F, Rivière-Lorphèvre E, Filippi E, Petit F, Preux N (2014) Trajectories in Laser Machining Ceramics: Thermal Model to Control Material Remove Rate. In: *Elev. Int. Conf. High Speed Mach., Czech Machine Tool Society*, Prague1–7.
[9] Rahman Chukkan J, Vasudevan M, Muthukumaran S, Ravi Kumar R, Chandrasekhar N (2015) Simulation of Laser Butt Welding of AISI 316 L Stainless Steel Sheet Using Various Heat Sources and Experimental Validation. *Journal of Materials Processing Technology* 219:48–59.
[10] Rosenthal D (1946) The theory of moving sources of heat and its application to metal treatments. *Transaction of ASME* 68:849–866.

Please cite this article as: F. Ducobu et al., Prediction of local sintering in laser beam machining of green Y-TZP ceramic, CIRP Annals - Manufacturing Technology (2020), https://doi.org/10.1016/j.cirp.2020.04.051